Journal of Polymers and the Environment (2021) 29:859–870
https://doi.org/10.1007/s10924-020-01920-7

ORIGINAL PAPER

Carboxymethyl Cellulose-Grafted Graphene Oxide/Polyethylene Glycol for Efficient Ni(II) Adsorption

Hebat-Allah S. Tohamy[1] · Mohamed El-Sakhawy[1] · Samir Kamel[1]

Accepted: 3 October 2020 / Published online: 15 October 2020

Abstract

Carboxymethyl cellulose-grafted graphene oxide blended with polyethylene glycol composite hydrogel as a new adsorbent was prepared. Firstly, graphene oxide was synthesized from sugarcane bagasse as a plentiful waste via a single-step oxidation under muffled atmospheric conditions. Furthermore, carboxymethyl cellulose was prepared from extracted cellulose and grafted onto graphene oxide by different ratios. The grafted graphene oxide was blended with polyethylene glycol in presence of glutaraldehyde as a cross linker to form a triple network hydrogel. The structures and morphologies of the prepared composite were characterized using Fourier transform infrared spectroscopy (FT-IR), X-ray diffraction (XRD), scanning electron microscopy (SEM) and TGA/DTA analysis. The prepared composites were used as adsorbents for the removal of Ni ions from aqueous solution. Different adsorption conditions were investigated such as; time intervals (15–90 min), Ni^{2+} concentrations (15–30 ppm), and temperature (298–328 K). The kinetics and isotherms were studied to highlight the adsorption rate and mechanism of the adsorption process. The results showed that the hydrogels fitted with the Langmuir isotherm model and the pseudo-second order with the best fit of R^2. On the other hand the positive values of ΔH, the negative values of ΔG, and the positive values of ΔS indicated that the Ni^{2+} adsorption is an endothermic process. The prepared hydrogels showed promising properties as the adsorption materials.

Keyword Graphene oxide · Carboxymethyl cellulose · Hydrogel · Ni^{2+} adsorption · Thermodynamic and kinetic studies

Introduction

Recently, scientists of environment considered the metals contamination of water is as an essential topic. Not only the water can be contaminated from natural sources like volcanoes, ore deposits, and weathering but also it can be contaminated from anthropogenic activities for example wastewater irrigation, agriculture activities, industries, and mining [1]. So, the contamination of water is a worldwide problem for the environment as well as human health [2].

Nanotechnology has opened a window of opportunity for researching water purification by new economically viable materials [2]. Nanomaterials, namely nanoparticles, graphene, graphene oxide, and carbon nanotubes have the capability to perform as adsorbents, which make it a good choice for the adsorption of water pollutants [2]. However, the high price of graphene and conventional adsorbent fostered researchers to focus on alternative adsorbent produced from lignocellulosic materials (i.e. eco-friendly materials) [2]. On the other hand, several technologies have been developed for the treatment of wastewater and the most concerning methods are electrolytic methods, membrane filtration, ion exchange, flotation, and chemical precipitation [3]. But the disadvantages of these techniques such as high cost, generation of other waste products, and low efficiency leads to noneconomic applications. Consequently, the researchers focus on eco-friendly systems such as the adsorption-based system especially using bioadsorbents. The adsorption processes depend on the adsorbent type, fluid properties, and pollutants to be removed as well as processing conditions [2].

In general, biodegradable and renewable polymer composites are called eco-friendly or green polymer composites. These polymer composites can be easily composted or disposed of without damaging the environment [2, 4]. Agricultural wastes are plentiful, eco-friendly materials, and can be easily recycled into valuable products to remove the

✉ Samir Kamel
samirki@yahoo.com

[1] Cellulose and Paper Department, National Research Centre, 33, El-Bohouth Str., Dokki, P.O. 12622, Giza, Egypt

pollutants from water. Cellulose is the major component of these wastes and it is formed by β-1,4-glycosidic linkages of the D-glucose unit that is the potential to become adsorbent material for metal ions. Cellulose can be used directly or after some modifications [5, 6]. Therefore, the chemical modifications can be carried out to enlarge the range of applications. A typical example is carboxymethyl cellulose (water-soluble) which also applied in this study. It is a nontoxic, hydrophilic, hetero-polysaccharide and can be used as a binder, rheology modifier, anti-redeposition aid, water thickener and to enhance product quality and stability [6, 7]. Also, polyethylene glycol as a biodegradable synthetic material is a biocompatible and nontoxic polymer. It is soluble in many organic solvents and water [8]. On the other hand, graphene oxide can be obtained by oxidation of agricultural waste like sugarcane bagasse in the presence of ferrocene (F) as an economic method [2]. So, composites consisting of carboxymethyl cellulose (CMC), graphene oxide (GO), and polyethylene glycol (PEG) have attracted great interest due to their biocompatibility and biodegradability. Consequently, this work deals with a win–win strategy to create new composite adsorbents based ecofriendly components. Firstly, GO was synthesized from sugarcane bagasse as agricultural waste and grafted by CMC followed by blending with PEG and crosslinked to give hydrogel.

Since batch reactor could be utilized for water treatment and it is useful to determine the adsorption rates, maximum adsorption capacities, and thermodynamic parameters [2]. The efficiency of the prepared hydrogels for the removal of Ni^{2+} from aqueous solutions has been investigated. Different parameters such as contact time and temperature as well as the initial ion concentrations were evaluated. The adsorption kinetics and isotherms were also investigated.

Experimental

Materials

Sugarcane bagasse was kindly provided by Quena Company for Paper Industry, Egypt. It was air-dried, homogenized to avoid compositional differences between batches, and ground to mesh size 450 micron. Ferrocene (F) was purchased from Sisco research laboratories Pvt. Ltd. Bleached Kraft bagasse pulp was obtained from Misr Edfu Pulp, Writing and Printing Paper Company (MEPP Co.), Egypt. The contents of the pulp, including α-Cellulose, Klason lignin, Hemicelluloses, and Ash were 77.60 ± 0.65, 0.87 ± 0.23, 21.40 ± 0.76, and 1.30 ± 0.41%, respectively. Polyethylene glycol (PEG, MWt 4000) was purchased from Alfa Aesar, Germany. Other used chemicals were of analytical grades and used without further purification.

Synthesis of Graphene Oxide (GO) from Sugarcane Bagasse (SCB)

Graphene oxide (GO) was prepared by oxidation of SCB in presence of ferrocien as described in our previous work and was approved by FT-IR, XRD, SEM and TEM spectrum [2].

Preparation of Carboxymethyl Cellulose (CMC)

In a typical procedure, to a suspended bleached pulp 15 g/400 ml isopropyl alcohol, 30% NaOH solution was added dropwise for 30 min and the mixture was left under stirring for 1 h at room temperature. After 1 h, 18 g of mono chloroacetic acid (MCA) dissolved in isopropyl alcohol was added dropwise to the mixture for 30 min. The mixture was allowed to react under stirring at 55 °C for 3.5 h. The liquid is drained off, and the fibrous product is stirred in 70% methanol, separated by filtration, and dried at 60 °C. The degree of substitution of the carboxyl group in CMC was assessed by potentiometric titration according to the standard method (DS ~ 0.7) [6].

Preparation of GO–Polyethylene Glycol–CMC Composite

0.1 g GO was added to a solution of CMC (5 g/200 ml H_2O)and ultrasonicated for 30 min. 5 ml of polyethylene glycol was added to the solution followed by 20 ml of glutaraldehyde solution in 1% HCl and continued stirring for 15 min. The composites were obtained by drying the mixture at 80 °C in an oven [8, 9].

A series of hydrogels were prepared to study the effect of cross linker. The samples were abbreviated by H_X (H_1, H_2, H_3, H_4, and H_5) as five different ratios of glutaraldehyde to CMC.

Characterization of Prepared Samples

Fourier transforms infrared (FTIR) spectroscopy was carried out using a Mattson 5000 spectrometer (Unicam, UK) by the KBr technique. In addition, the samples were investigated using scanning electron microscopy (SEM), Quanta 250 FEG. Atomic absorption PerkinElmer 3110, USA was used to quantify the amount of metal ions.The crystallinity was analyzed using X-ray diffraction. Diffraction patterns were obtained using a Bruker D8 Advance X-ray diffractometer (Germany). The diffraction patterns were recorded at a voltage of 40 kV with a current of 40 mA, using copper (K_α) radiation (1.5406 Å). Scans were taken over a 2θ (Bragg angle) range from 5 to 80°.

The thermal activity between ~ 25 and 900 °C was studied on PerkinElmer STA 6000 with a nitrogen gas flow rate of 50 ml/min and at a 10 °C/min heating rate. Thermogravimetric analysis data (TA/DTA) can be investigated to calculate the activation energy (Ea) of the thermal degradation process. The general correlation equations used in the Coats–Redfern method are:

$$\log\left[\frac{1-(1-\alpha)^{1-n}}{T^2(1-n)}\right] = \log\frac{AR}{\beta E}\left[1-\frac{2RT}{E}\right] - \frac{E}{2.303RT} \text{ for } n \neq 1 \quad (1)$$

$$\log\left[\frac{-\log(1-\alpha)}{T^2}\right] = \log\frac{AR}{\beta E}\left[1-\frac{2RT}{E}\right] - \frac{E}{2.303RT} \text{ for } n = 1 \quad (2)$$

where α is the fractional conversion, n is the order of degradation reaction, R is the gas constant (in kJ/mol K), T is the temperature (in K), A is the frequency factor (s^{-1}), β is the heating rate (K/min) and E is the activation energy. From the above equation, plotting the left hand side of Eqs. (1), (2) against 1/T using different n values should offer a straight line, with the most proper value of n. Thus, the method of least squares was applied for the equation, taking various n values (from 0 to 3.0) and calculating for each value of *n*, the correlation coefficient (R^2) and standard error estimation (SE). The activation energies were estimated from the slope (E/2.303R), while *A* was estimated from the intercept (log AR/β E) of the Coats–Redfern equation with the most proper value of *n* [7, 10]. The other kinetic parameters; the enthalpy of activation (ΔH), the entropy of activation (ΔS), and the free energy change of activation (ΔG) were calculated using the relationships:

$$\Delta H^* = E^* - RT;\ \Delta G^* = \Delta H^* - T\Delta S^* \text{ and } \Delta S^* = 2.303\left(\log\frac{Ah}{RT}\right)R \quad (3)$$

where (*k*) and (*h*) are Boltzman and Planck constants, respectively [11].

Adsorbents Comparative Study

The metal ions can bind to the most cellulosic materials by electrostatic interaction as a result of simultaneous ionic exchange and complexation. The removal of Ni^{2+} from water by hydrogel as adsorbents is determined by the nature of the functional groups, the amounts present, and the sorption conditions as the time, temperature, and initial metal ion concentration [12]. To characterize the sorption efficiency of differently prepared hydrogel adsorbents toward the removal of Ni^{2+} from water. A comparative removal efficiency (R) of these adsorbents were studied at different contact times and temperatures with different concentrations of Ni^{2+} [2]. R was calculated using the following equation:

$$R = \frac{(C_0 - C_1)}{C_0} \times 100\% \quad (4)$$

where C_0 and C_t are the Ni^{2+} concentrations (mg/L) in solution before and after adsorption respectively, V is the solution volume (L) and M is the amount (g) of the sorbent employed in the adsorption experiment [2].

Kinetic Modeling

In order to achieve the controlling rate mechanism of the adsorption processes such as mass transfer and chemical reaction, the pseudo-first-order and pseudo-second-order equations are utilized to model the kinetics data of Ni^{2+} adsorption onto different samples [2]. The first and second-order equations were applied to the data derived from the effect of time on adsorption [2].

(i) Pseudo first-order is based on the hypothesis that physisorption is the rate-determining step and it is given in Eq. (5).

$$\ln\,[qe - qt] = \ln\ qe - K1t \quad (5)$$

where qe and qt are the amounts of Ni^{2+} adsorbed (mg/g) at equilibrium sorption capacity and time t respectively, K_1 (min^{-1}) is the Pseudo first order rate constant of adsorption [2].

(ii) Pseudo second-order is based on the hypothesis that chemisorptions is the rate determining step and it is given in Eq. (6).

$$\frac{t}{qt} = \frac{1}{K2qe2} + \frac{t}{qe} \quad (6)$$

where K_2 (g/mg/min) is the rate constant of Pseudo-second order adsorption. Values of qe_2 and K_2were calculated from the slope and intercept of the plot of t/qt against t [2].

Adsorption Isotherm

Adsorption isotherm studies the distribution of adsorbed molecules between the liquid and the solid phases at equilibrium state. This means studies the adsorption mechanisms, the surface properties, and affinities of the adsorbent. R^2 is used to determine the best-fitting isotherm [2].

Langmuir Isotherm Model:

It is the simplest type and base on the vision that every adsorption sites are equivalent and independent [2].

$$\frac{Ce}{qe} = \frac{1}{Kqm} + \frac{Ce}{qm} \quad (7)$$

where q_m (mg/g) is the maximum removal capacity [2].

(i) The Freundlich model. It describes the non-ideal and reversible adsorption and prefers to represent heterogeneous materials better than other models [2].

$$\log qe = \log Kf + \frac{1}{n} \log Ce \quad (8)$$

where K_f is adsorption capacity [2].

Langmuir isotherm restricted to the formation of the monolayer in contrast to Freundlich isotherm which can be applied to multilayer adsorption, with a non-uniform distribution of adsorption heat and affinities over the heterogeneous surface [2].

Thermodynamic Parameters

The speed of the reaction can be calculated from the awareness of kinetic studies. But the change in a reaction that can be expected during the process needs a brief idea of thermodynamic parameters [13].

Thermodynamic parameters such as the Gibbs free energy (ΔG, kJ/mol), enthalpy (ΔH, kJ/mol), and entropy (ΔS, kJ/mol) change during the adsorption process and can be estimated from the equation of Van't Hoff [14, 15]:

$$\ln Kd = \frac{\Delta S}{R} - \frac{\Delta H}{RT} \quad (9)$$

where T is the temperature in Kelvin, and R is the universal gas constant (8.314 $Jmol^{-1}\ T^{-1}$) [16]. The distribution coefficient (K_d) can be calculated using the equation [15]:

$$K_d = \frac{Ci - Ce}{Ce} \times \frac{v}{m} \quad (10)$$

The Gibbs free energy can be calculated using the equation:

$$\Delta G = -RT \ln K_d \quad (11)$$

The values of ΔH and ΔS can be obtained from the slope and intercept of Van't Hoff plot of lnK versus 1/T [17, 18].

Results and Discussion

Preparation and Characterization of Adsorbent Hydrogel

The adsorbent hydrogel was prepared by ultrasonic dispersion, followed by freeze-drying, as shown in Fig. 1a.

The schematic diagram of the hydrogen bonding interaction of composite system was shown in Fig. 1b.

FT-IR Analysis

The chemical structure of GO, CMC, CMC/PEG, and their composite was confirmed by Fourier-transform infrared spectroscopy (Fig. 2). The FT-IR spectrum demonstrates the characteristic peaks of GO at 3425, 2991, 1716, 1617, 1469, 1194, and 904 cm^{-1} which attributed to OH, C-H, C = O, C = C, O-C = O, C–O–C, and C-O respectively [2]. The characteristic bands of CMC at 3422, 1606, and 1061 cm^{-1} correlated to the stretching -OH, -COONa, and C–O–C stretching [6].

The FTIR spectra of CMC/PEG and their composite with GO have differed from that of GO and CMC as evidenced by the dramatic decrease in the intensities of the characteristic peaks of oxygen functionalities (ν_{O-H}, and $\nu_{C=O}$).

Since the band at 2991 cm^{-1} is attributed to C-H stretching, this band can be chosen as an internal standard to determine the relative absorbance (RA) [2, 4, 6]. The RAs of the O–H were 3.20, 2.66, 1.26, and 1.28, while, the RAs of the C = O were 14.70, 1.14, 1.99, and 1.77 for GO, CMC, CMC/PEG, and their composite respectively. And it is clear that the RAs of the O–H and C = O groups strongly decreased compared to that of GO. This means that the cross-linking reaction takes place between the OH group of GO, CMC, and PEG [2, 4, 6].

The absorbance intensities at 1420–1430 and 900 cm^{-1} are characterized by the amount of crystalline and amorphous structure of the materials, respectively, and the ratio between them was defined as the empirical crystallinity index [5]. Upon grafting of CMC and PEG on GO, the empirical crystallinity index (LOI) of GO decreased due to the transformation of crystalline regions in GO to amorphous one by grafting as the layers of GO before grafting are still compact, compared to exfoliated one [19]. Also, the OH stretching vibration of GO (3441 cm^{-1}) was shifted to a lower frequency after grafting of CMC and PEG on GO and this may be due to intermolecular hydrogen bonding [6]. The schematic diagram of the hydrogen bonding interaction of hydrogel was shown in Fig. 1B.

Scanning Electron Microscopy (SEM)

The surface morphology of an adsorbent is one of the most important factors governing the adsorption process. Scanning electron microscopy was used to investigate the surface morphology of composite and its components (Fig. 3). GO sheets are clearly visible in Fig. 3a and resembles rounded folds, a cloud, and a sheet-like structure with a flat surface. While CMC has a micro-sized fibrous structure Fig. 3b and CMC/PEG shows a more porous structure compared to GO and CMC Fig. 3c. SEM image of composite has been shown in Fig. 3d. As shown in the SEM image of composite, the surface morphology showed a rough structure and severe

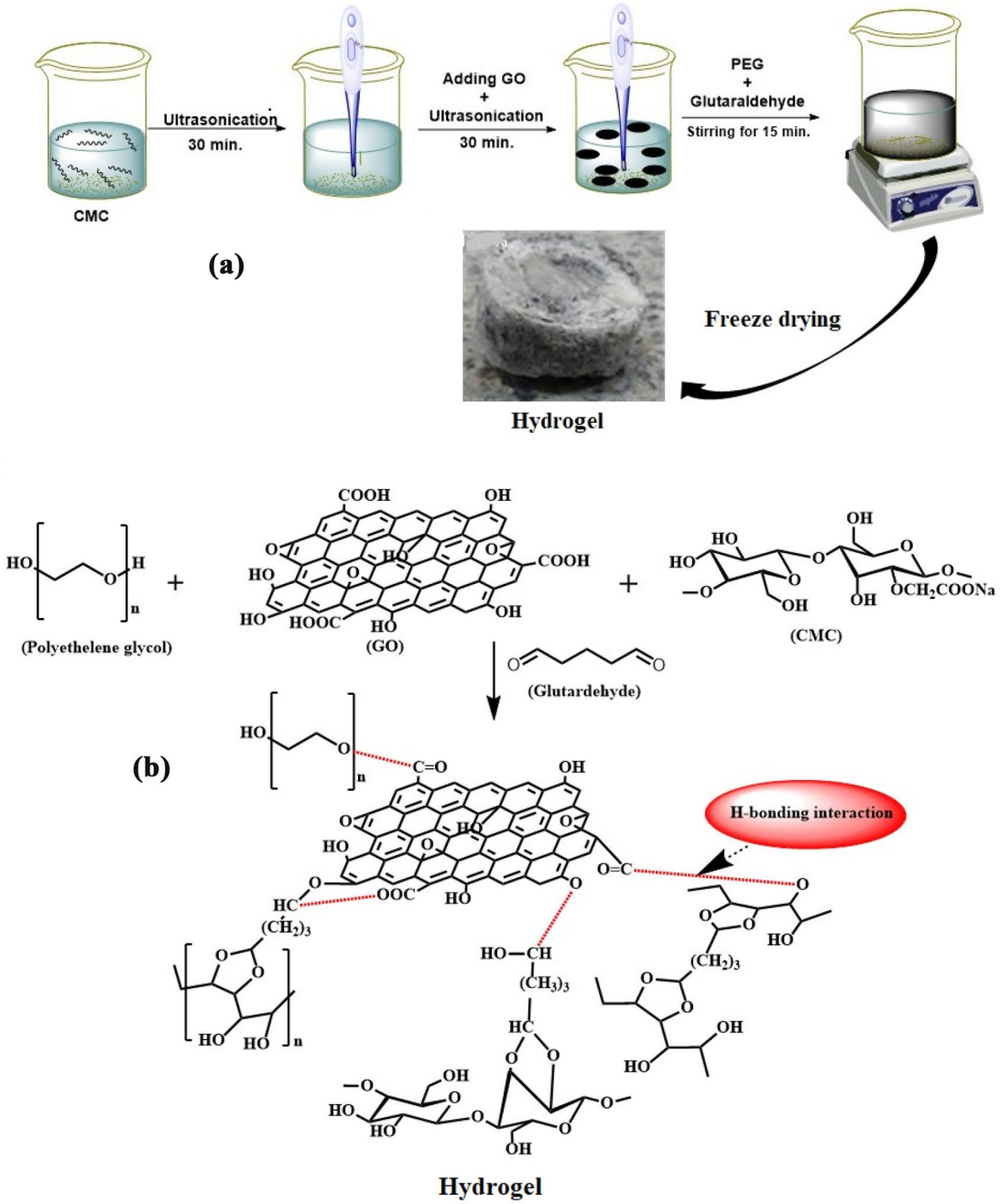

Fig. 1 **a** Preparation process of adsorbent hydrogel via freeze drying and **b** anchoring effect of PEG and CMC molecules into GO surface

wrinkles and uniform dispersion of GO in the polymer matrices.

XRD Analysis

To obtain information about the crystalline structure of the prepared composite, the XRD patterns of the GO, CMC/PEG, and their composite are shown in Fig. 4. GO has a characteristic diffraction peak at $2\theta = 9.3°$ related to (001) plane, with the interlayer spacing of 0.48 nm and at $2\theta = 21.8°$ related to (002) plane due to the incomplete oxidation process [20, 21]. The observed two peaks at 44.4° and 72.2° are attributed to reflections from the aluminum holder used. The CMC/PEG has a broad diffraction peak at $2\theta = 21.4°$, and other at $2\theta = 30.3°$ that are characteristic of CMC and indicating that the CMC is partly crystalline [4]. In the XRD profile of composite, the intensity of diffraction peaks of CMC decreased. The intensity of peak at $2\theta = 9.4°$

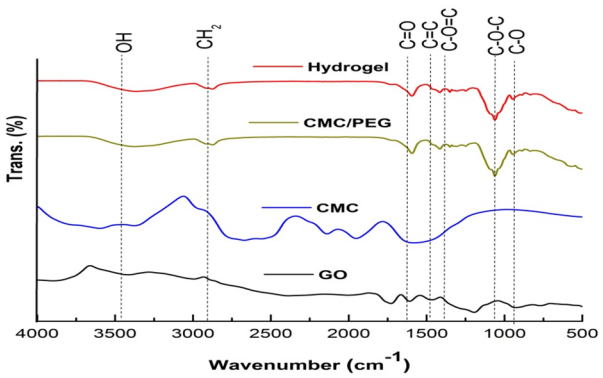

Sample	GO	CMC	CMC/PEG	Composite
LOI	1.14	0.17	0.75	0.52

Fig. 2 FT-IR spectrum andcrystallinity index of GO, CMC, CMC/PEG, and their composite

decreased, which is characteristic for the GO with interlayer spacing ($d_{spacing}$) of 0.52 nm. The decreasing of the crystallinity index of GO after the grafting reaction due to cleavage of the hydrogen bonds, which diminishes the crystallinity and this coincides with the mean hydrogen bond values calculated from the FTIR spectra [4].

Thermal Properties

Figure 5 displays the thermogravimetric analysis curves of GO, CMC/PEG, and their composite and it is clear that; the thermal behavior of these materials was highly different. TGA curves revealed three decomposition steps for GO, while CMC/PEG and composite have four decomposition steps. A sudden change in temperature generates a thermal shock and functionalities are taken out from the GO lattice as water vapor, CO, and CO_2. The evolution of gases generates pressure between two GO stacked layers which is the key factor for exfoliation [7, 10]. The residual weights of GO, CMC/PEG, and their composite were 23.20, 19.96, and 27.64% at 800, and 1000 °C respectively, which indicated the presence of a fraction of non-volatile components.

It is interesting to note that, the shape of thermogram curves changes in the case of CMC/PEG, and composite. Where, the 2nd degradation stage is split into two stages

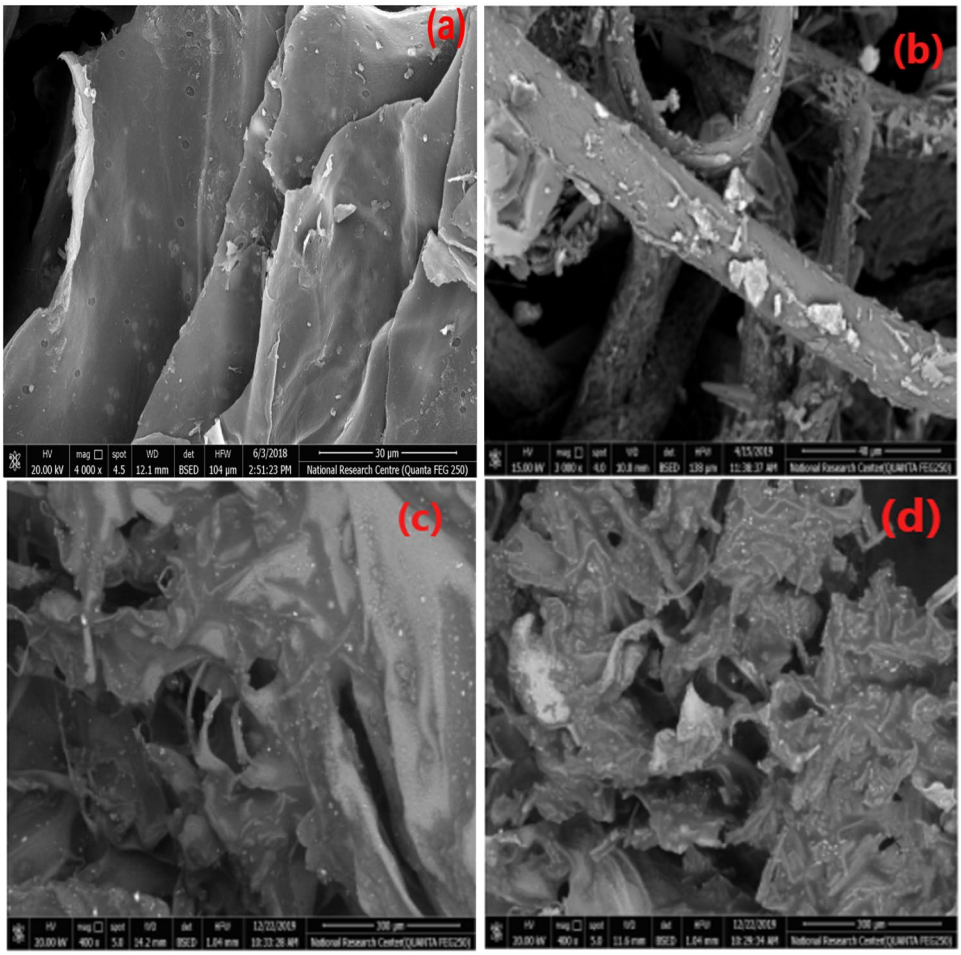

Fig. 3 SEM of **a** GO, **b** CMC, **c** CMC/PEG, and **d** and their composite

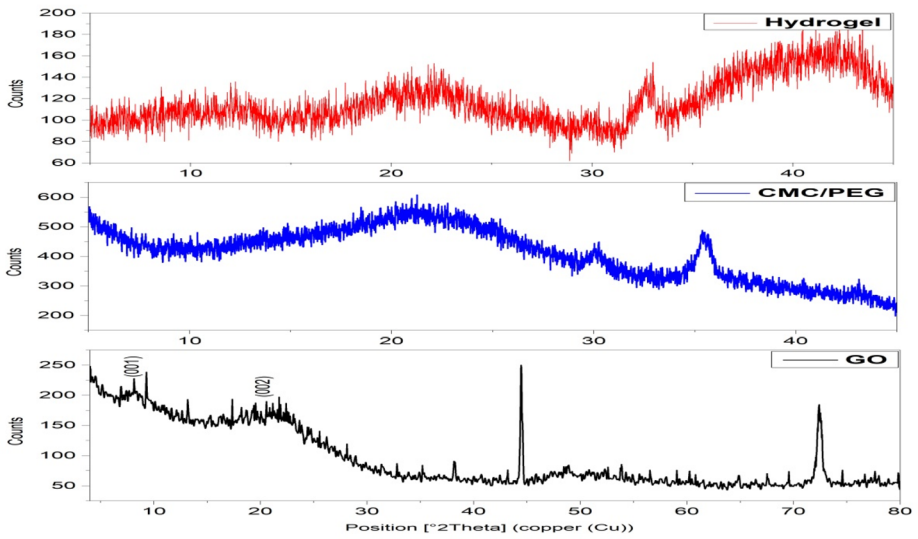

Fig. 4 X-ray patterns and crystallinity index of; GO, CMC/PEG, and their composite

Sample	GO	CMC/PEG	Composite
CrI. (%)	41.75	37.21	24.49

with the peak maxima 289.1 and 328.4 °C, and 292.1 and 336.0 °C for CMC/PEG, and composite respectively, which indicates the relatively lower thermal stability of CMC/PEG, and composite than GO. The 3rd decomposition step between 724.9–989.1 and 746.3–986.6 °C, with a maximum at 787.8 and 814.2 °C (average weight loss of 12.84 and 11.49%), which was ascribed to the decomposition of the carbonaceous residues to form low molecular weight gaseous products [7, 10]. Finally, the TGA results imply that the mobility of the polymer segments in GO was suppressed by the strong hydrogen bonding interactions between them, resulting in a delay in the polymer degradation [10]. Overall, the thermal stability of the CMC/PEG, and the composite has been decreased compared to that of pure GO, confirming the grafting structural changes. GO has higher thermal stability probably due to more ordered, H-bonded and packed unexfoliated graphene sheets, this in turn possibly increasing the thermal decomposition temperature of GO [2, 10].

Effect of Contact Time

Figure 6 illustrates the course of absorption at room temperature using differently prepared hydrogel adsorbents in the range of 15–90 min with 15 mg/L as an initial concentration of Ni^{2+} and adsorbent dosage 20 mg. In the beginning period, the removal efficiency (R%) were very marked and reached the equilibrium stage at the initial stage (30–45 min) due to the presence of more active sites [2]. This means a contact time of 30–45 min was sufficient to ensure saturation with a maximum q and R%. The delay in the time of adsorption may be attributed to the weakening of the driving force resulting in the decrease of available adsorption sites. These decreased as a result of releasing H^+ from the oxygen-containing functional groups (e.g. COOH or OH) on the surface of hydrogel to the solution, hence delaying adsorption [8]. The difference in the adsorption attitude of Ni^{2+} by the prepared samples proves that the samples are different in their morphology (Fig. 6).

Effect of Temperature

The effect of temperature on the adsorption capacity of Ni^{2+} on hydrogels was performed from 298 to 328 K with an initial concentration of Ni^{2+} of 15 mg/l and adsorbent dosage 20 mg for 30 min. As shown in Fig. 6, the sorption capacity (q) and removal efficiency (R%) sharply increased from 298 to 328 K. No more adsorption was noticed by increasing adsorption temperature so, it can be concluded that no further benefits can be obtained from increasing the temperature during the adsorption process. This indicates that the adsorption of Ni^{2+} by the prepared hydrogel is an endothermic process [2]. This can be explained as increasing the temperature increases the rate of diffusion of Ni^{2+} across the external boundary layer and in the internal pores. Al-Senai et al. suggested that the adsorption of Ni^{2+} ions by GO derivatives may involve physical and chemical adsorption due to higher temperatures, lead to an increase in active sites due to the bond rupture [2]. While Dawodu et al. explained the endothermic adsorption

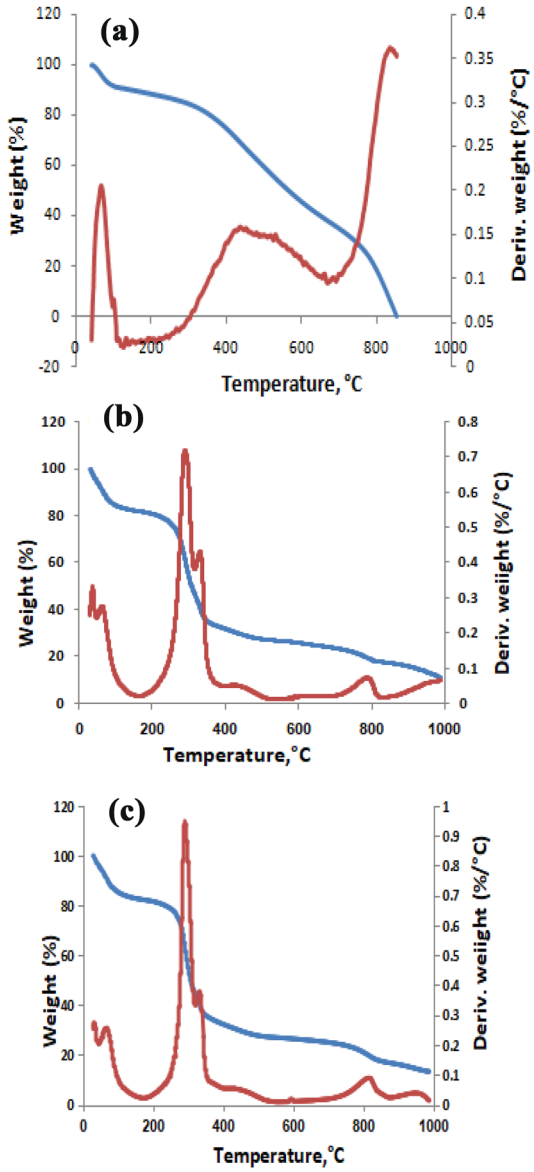

Fig. 5 TGA, and DTA curves and TGA data of; **a** GO, **b** CMC/PEG, and **c** composite

Sample	Weight loss at 1000 °C, %	Residual weight, %	Temp. of steps in TGA, °C			
			Step 1	Step 2	Step 3	Step4
GO	76.80	23.2	64.6	431.7	836.3	-
CMC/PEG	80.04	19.96	64.3	289.1	328.4	787.8
Composite	72.26	27.74	71.2	292.1	336.0	814.2

process by the enlargement of pore size and activation of GO surface [2].

Effect of Initial Concentration

The effect of the initial concentration of Ni^{2+} solution on the amount of adsorbed Ni2 + by the prepared hydrogels was performed using various concentrations (15, 20, 25, and 30 mg/L) with adsorbent dosage 20 mg at 25 °C for 30 min. From Fig. 6, Ni^{2+} uptake increased with increasing of the Ni^{2+} concentration up to 20 mg/L for H5 and H7.5 and up to 25 for other hydrogels. Further increase of the Ni^{2+} ions concentration was found to have no effect. This behavior may be due to the consumption of all the exchange centers with Ni^{2+} ions using 20 and 25 mg/L [2]. Or maybe due to that the initial concentration delivers an important driving force to overcome all mass transfer resistances between the solid and liquid phases [22]. But after a definite concentration, the Ni^{2+} adsorption begins

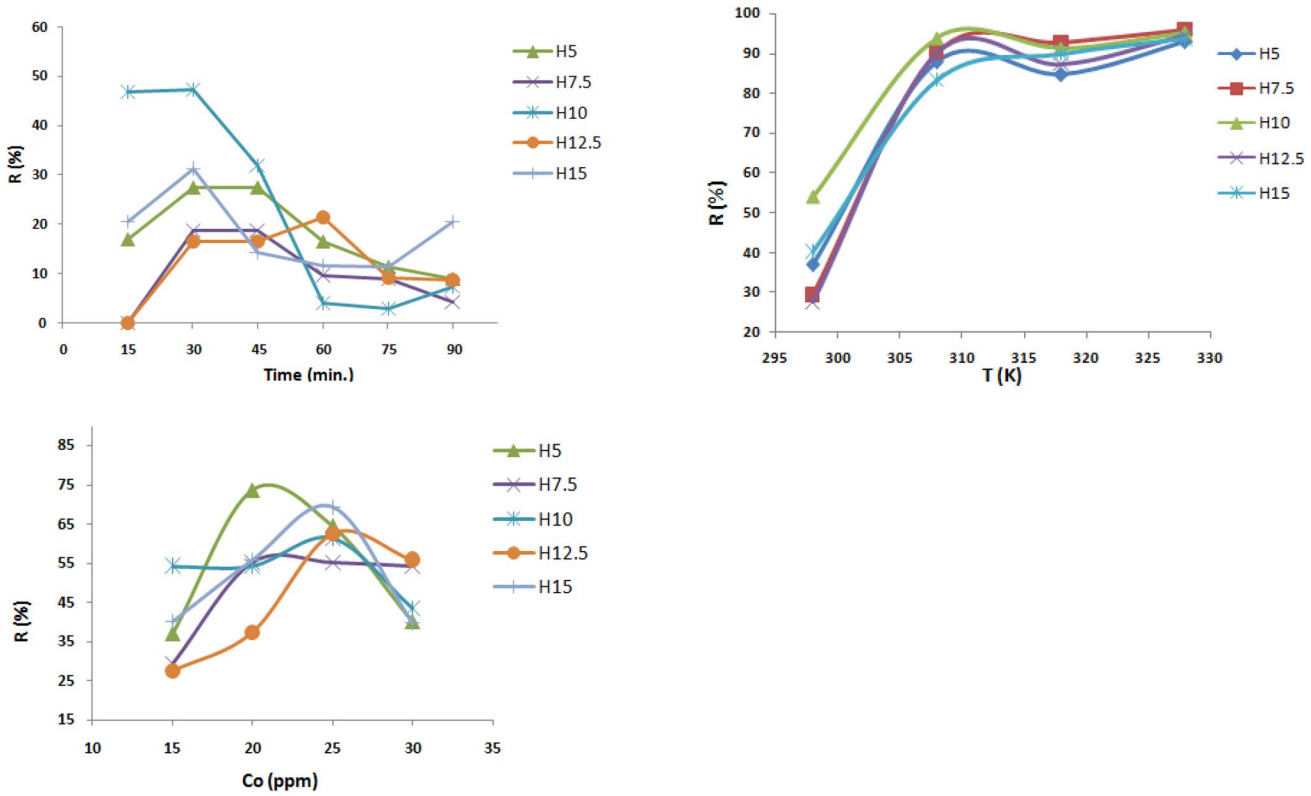

Fig. 6 Effect of; contact time, temperature, and the initial Ni^{2+} concentration on the adsorption process by the prepared composite

to decrease the lack of sufficient surface area to accommodate the excess of Ni^{2+} [2].

Kinetic Modeling

Figure 7a and b represents the kinetic parameters of the Pseudo-first-order and Pseudo-second-order reactions for adsorption of Ni^{2+} onto the prepared composite at different time intervals. Concerning the values of R^2 presented in Table 1, it is seen that the pseudo-second-order model gave a better fit to the adsorption data than the first-order one for all samples. The values obtained in the Pseudo-first-order are still suitable for describing the kinetics of Ni^{2+} sorption. This elucidates that the surface processes involving chemisorptions and physisorption participate in the adsorption of Ni^{2+} by the prepared hydrogels [2].

Adsorption Isotherm

All isotherms (Fig. 7c and d) best fit the Langmuir model so, it can be derived that the surfaces of hydrogels are homogeneous, and surface adsorption is often done in the form of the monolayer [2] (Table 2).

Thermodynamic Parameters

The positive value of ΔH in the prepared hydrogels is due to the endothermic process (i.e. the adsorption capacity increases with increasing temperature) [23]. The negative values of ΔG indicate that the sorption process is spontaneous [24]. The ΔS changes in this study are found to be positive; it means that the increased randomness appeared on the solution interface during the exchange of Ni^{2+} (Table 3) [25].

Conclusion

A novel approach toward the production of a new adsorbent hydrogel by grafting of carboxymethyl cellulose onto graphene oxide and blended with polyethylene glycol in presence of glutaraldehyde as a cross-linker was reported. Our findings hinted that the interaction between Ni^{2+} and adsorbent hydrogel is an endothermic process (with a positive value of ΔH). The results of kinetic modeling, adsorption isotherms, and thermodynamic parameters show three things. First, the pseudo-first and second-order models gave a better fit to the adsorption of the adsorbent hydrogel.

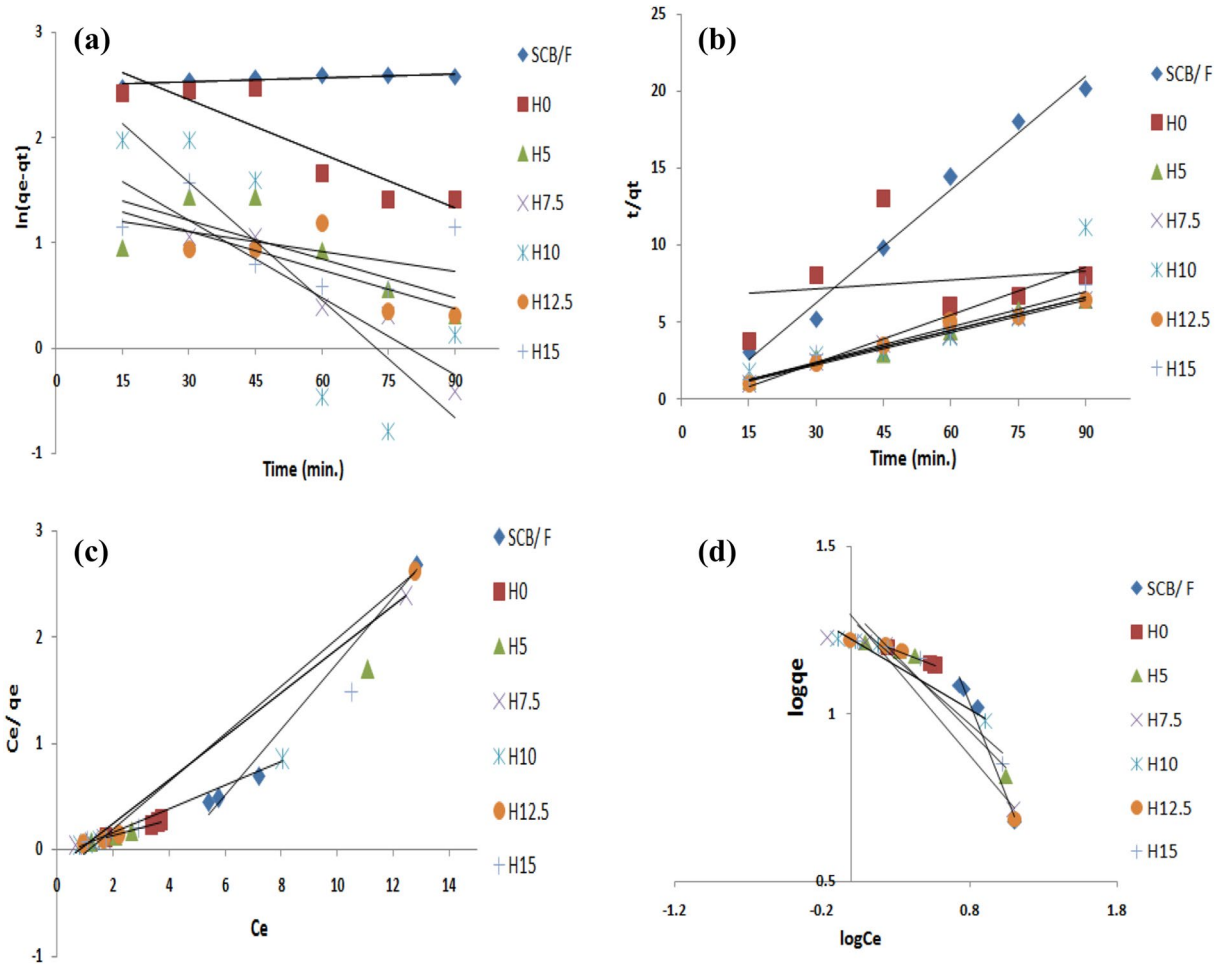

Fig. 7 Kinetic parameters of **a** Pseudo-first-order and **b** pseudo-second-order reaction for adsorption of Ni^{2+} onto the prepared composite at different time intervals (Upper). **c** Langmuir isotherm and **d** Freundlich isotherm of Ni^{2+} onto the prepared composite (Lower)

Table 1 Comparison between the estimated adsorption rate constants, rate constants and correlation coefficients associated with the pseudo-first-order and the pseudo-second-order rate

Kinetic model	Parameter	Adsorbent				
		H5	H7.5	H10	H12.5	H15
Pseudo first order	q_{exp}	4.84	7.03	14.83	4.41	3.64
	q_{calc}	4.22	2.87	7.24	3.28	4.78
	K_1	0.012	0.024	0.037	0.012	0.006
	R^2	0.560	0.904	0.689	0.553	0.197
Pseudo second order	q_{calc}	14.06	14.24	9.60	13.84	13.17
	K_2	0.037	0.49	0.137	0.470	0.471
	R^2	0.973	0.987	0.756	0.980	0.977

Table 2 Langmuir and Freundlich models parameters for adsorption of Ni^{2+} onto hydrogels

Kinetic model	Parameter	Adsorbent				
		H5	H7.5	H10	H12.5	H15
Langmuir	q_m (mg/g)	5.84	4.85	8.97	4.44	6.43
	R^2	0.994	0.997	0.998	0.996	0.991
Freundlich	K_f ($mg^{(1-1/n)}$ g^{-1} $L^{1/n}$)	3.71	3.42	3.40	3.64	3.61
	R^2	0.930	0.932	0.966	0.933	0.910

Table 3 Thermodynamic parameters for hydrogels adsorption of Ni^{2+}

Parameter	Adsorbent				
	H5	H7.5	H10	H12.5	H15
ΔS (kJ/mol)	0.25	0.35	0.23	0.30	0.27
ΔH (kJ/mol)	74×10^3	103×10^3	67×10^3	91×10^3	81×10^3
ΔG (kJ/mol)					
298 K	1.31	2.17	− 0.42	2.39	0.98
308 K	− 5.09	− 5.71	− 7.03	− 5.71	− 4.13
318 K	− 4.53	− 6.81	− 6.24	− 5.14	− 5.80
328 K	− 7.04	− 8.75	− 8.24	− 7.75	− 7.39

Second, isotherms best fit the Langmuir model. Third, the negative values of ΔG indicate that the sorption process is spontaneous.

Acknowledgements The authors acknowledge the Academy of Scientific Research and Technology (ASRT), Egypt (grant ASRT-19-06) for financial support of the bilateral research activities.

Compliance with Ethical Standards

Conflict of interests The authors declare that they have no known competing financial interests or personal relationships that could have appeared to influencethe work reported in this paper.

References

1. Kamal KH, Dacrory S, Ali SS, Ali KA, Kamel S (2019) Adsorption of Fe ions by modified carrageenan beads with tricarboxy cellulose: kinetics study and four isotherm models. Desalin Water Treat 165:281–289. https://doi.org/10.5004/dwt.2019.24560
2. Tohamy H-AS, Anis B, Youssef MA, Abdallah AEM, El-Sakhawy M, Kamel S (2020) Preparation of eco-friendly graphene oxide from agricultural wastes for water treatment. Desalin Water Treat 191:250–262. https://doi.org/10.5004/dwt.2020.25652
3. Kamel S, El-Gendy AA, Hassan MA, El-Sakhawy M, Kelnar I (2020) Carboxymethyl cellulose-hydrogel embedded with modified magnetite nanoparticles and porous carbon: effective environmental adsorbent. Carbohydr Polym 242:116402. https://doi.org/10.1016/j.carbpol.2020.116402
4. El-Sakhawy M, Kamel S, Salama A, Tohamy H-AS (2018) Preparation and infrared study of cellulose based amphiphilic materials. Cellul Chem Technol 52:193–200
5. El-Sakhawy M, Kamel S, Salama A, Youssef M, Elsaid W, Tohamy H (2017) Amphiphilic cellulose as stabilizer for oil/water emulsion. Egypt J Chem 60(2):181. https://doi.org/10.21608/ejchem.2017.544.1002
6. El-Sakhawy M, Salama A, Kamel S, Tohamy H-AS (2018) Carboxymethyl cellulose esters as stabilizers for hydrophobic drugs in aqueous medium. Cellul Chem Technol 52(9–10):749–757
7. El-Sakhawy M, Tohamy H-AS, Salama A, Kamel S (2019) Thermal properties of carboxymethyl cellulose acetate butyrate. Cellul Chem Technol 53(7–8):667–675
8. Serag E, El-Nemr A, El-Maghraby A (2017) Synthesis of highly effective novel graphene oxide-polyethylene glycol-polyvinyl alcohol nanocomposite hydrogel for copper removal. J Water Environ Nanotechnol 2(4):223–234. https://doi.org/10.22090/JWENT.2017.04.001
9. Moharram M, Ereiba K, El Hotaby W, Bakr A (2015) Synthesis and characterization of graphene oxide/crosslinked chitosan nanaocomposite for lead removal form aqueous solution. Res J Pharm Biol Chem Sci 6(4):1473–1489
10. Tohamy HAS, Anis B, Youssef MA, Abdallah AE, El-Sakhawy M, Kamel S (2020) Thermal properties of graphene oxide prepared from different agricultural wastes. Egypt J Chem. https://doi.org/10.21608/EJCHEM.2020.22915.2375
11. Adel AM, Abd El-Wahab ZH, Ibrahim AA, Al-Shemy MT (2011) Characterization of microcrystalline cellulose prepared from lignocellulosic materials. Part II: physicochemical properties. Carbohydr Polym 83(2):676–687. https://doi.org/10.1016/j.carbpol.2010.08.039
12. Kamel S, Abou-Yousef H, El-Sakhawy M (2004) Copper (II) ions adsorption onto cationic oxycellulose. Energy Educ Sci Technol 14:51–60
13. Keleşoğlu S (2007) Comparative adsorption studies of heavy metal ions on chitin and chitosan biopolymers. İzmir Institute of Technology. https://hdl.handle.net/11147/3365.
14. Amin MT, Alazba AA, Amin MN (2017) Absorption behaviours of copper, lead, and arsenic in aqueous solution using date palm fibres and orange peel: kinetics and thermodynamics. Pol J Environ Stud. https://doi.org/10.15244/pjoes/66963
15. Mengistie AA, Rao TS, Rao AP, Singanan M (2008) Removal of lead (II) ions from aqueous solutions using activated carbon from *Militia ferruginea* plant leaves. Bull Chem Soc Ethiop. https://doi.org/10.4314/bcse.v22i3.61207
16. Payne KB, Abdel-Fattah TM (2004) Adsorption of divalent lead ions by zeolites and activated carbon: effects of pH, temperature, and ionic strength. J Environ Sci Health Part A 39(9):2275–2291
17. Al-Senani GM, Al-Fawzan FF (2018) Adsorption study of heavy metal ions from aqueous solution by nanoparticle of wild herbs. Egypt J Aquat Res 44(3):187–194. https://doi.org/10.1016/j.ejar.2018.07.006
18. Elmoubarki R, Mahjoubi F, Tounsadi H, Moustadraf J, Abdennouri M et al (2015) Adsorption of textile dyes on raw and decanted Moroccan clays: kinetics, equilibrium and thermodynamics. Water Resour Ind 9:16–29. https://doi.org/10.1016/j.wri.2014.11.001
19. Liu Q, Zhou X, Fan X, Zhu C, Yao X, Liu Z (2012) Mechanical and thermal properties of epoxy resin nanocomposites reinforced

with graphene oxide. Polym Plast Technol Eng 51(3):251–256. https://doi.org/10.1080/03602559.2011.625381
20. Kazemnejadi M, Mahmoudi B, Sharafi Z, Nasseri MA, Allahresani A, Esmaeilpour M (2019) Synthesis and characterization of a new poly α-amino acid Co (II)-complex supported on magnetite graphene oxide as an efficient heterogeneous magnetically recyclable catalyst for efficient free-coreductant gram-scale epoxidation of olefins with molecular oxygen. J Organomet Chem 896:59–69. https://doi.org/10.1016/j.jorganchem.2019.05.030
21. Tran HV, Tran TL, Le TD, Le TD, Nguyen HM, Dang LT (2018) Graphene oxide enhanced adsorption capacity of chitosan/magnetite nanocomposite for Cr (VI) removal from aqueous solution. Mater Res Express 6(2):025018. https://doi.org/10.1016/j.jorganchem.2019.05.030
22. Marzbali MH, Esmaieli M, Abolghasemi H, Marzbali MH (2016) Tetracycline adsorption by H3PO4-activated carbon produced from apricot nut shells: a batch study. Process Saf Environ Prot 102:700–709
23. Thajeel AS (2013) Isotherm, kinetic and thermodynamic of adsorption of heavy metal ions onto local activated carbon. Aquat Sci Technol 1(2):53–77. https://doi.org/10.1016/j.psep.2016.05.025
24. Lee I-H, Kuan Y-C, Chern J-M (2007) Equilibrium and kinetics of heavy metal ion exchange. J Chin Inst Chem Eng 38(1):71–84. https://doi.org/10.5296/ast.v1i2.3763
25. Kumar PS, Kirthika K (2009) Equilibrium and kinetic study of adsorption of nickel from aqueous solution onto bael tree leaf powder. J Eng Sci Technol 4(4):351–363. https://doi.org/10.1016/j.jcice.2006.11.001